Applied Catalysis B: Environmental 96 (2010) 370–378

Contents lists available at ScienceDirect

Applied Catalysis B: Environmental

journal homepage: www.elsevier.com/locate/apcatb

On the importance of the catalyst redox properties in the N_2O decomposition over alumina and ceria supported Rh, Pd and Pt

S. Parres-Esclapez, M.J. Illán-Gómez, C. Salinas-Martínez de Lecea, A. Bueno-López*

Inorganic Chemistry Department, University of Alicante, Ap. 99, E-03080 Alicante, Spain

ARTICLE INFO

Article history:
Received 21 December 2009
Received in revised form 21 February 2010
Accepted 24 February 2010
Available online 3 March 2010

Keywords:
N_2O decomposition
Noble metal catalyst
Ceria support
Cerium–praseodymium
Cerium–lanthanum

ABSTRACT

Rh, Pd and Pt have been supported on γ-Al_2O_3, pure CeO_2 and La- or Pr-doped CeO_2, and these catalysts have been tested for N_2O decomposition. The effect of CO and O_2 in the feed has been studied. The characterisation techniques used were Raman spectroscopy, XRD, N_2 adsorption at −196 °C, H_2-TPR and TEM. The catalytic activity for N_2O decomposition of the noble metals follows the trend Rh > Pd > Pt, and the support affects significantly the activity. For CeO_2-containing catalyst, a relationship between N_2O decomposition capacity and H_2 reduction of ceria has been found, the easier is the reduction the higher is the catalytic activity. The rate-limiting step of the N_2O decomposition mechanism over noble metal/ceria catalysts seems to be the reduction of the catalytic active sites. For Rh catalysts, ceria supports are involved actively in the decomposition of N_2O, and all the ceria-based supports improve the catalytic activity of Rh with regard to γ-Al_2O_3 due to the redox properties of ceria. The Pd catalysts with pure and doped ceria support showed similar activity, this being higher than that of Pd/γ-Al_2O_3. Pt/CeO_2 is the most active catalyst among those of Pt, but ceria doping by La or Pr has a negative effect on the activity. The most active catalyst among those prepared in this study is Rh/CeO_2(Pr).

1. Introduction

N_2O is the major source of NO_x in the stratosphere and contributes to the greenhouse effect and global warming. In the last decade, the relevance of N_2O abatement has been reflected in the literature [1–5]. Some anthropogenic sources of N_2O are nitric acid plants, fossil fuels and biomass combustion and land cultivation [1]. In addition, certain catalytic converters introduced for gas pollution control in vehicles also contribute to N_2O emission. Three Way Catalysts (TWC) used in gasoline-powered engines for CO, hydrocarbons (HC) and NO_x removal yield N_2O as by-product, and the undesired formation of N_2O has been related with the TWC aging. TWC combine noble metals, mainly Pt, Pd and/or Rh, with CeO_2-based materials [6,7] to promote the noble metal dispersion, increase the thermal stability of the Al_2O_3 support, promote the water gas shift (WGS) and steam reforming reactions, favour the catalytic activity at the interfacial metal-support sites, promote CO removal and store and release oxygen under, respectively, lean and rich conditions.

The main reactions occurring in a TWC are

$$CO + (1/2)O_2 \rightarrow CO_2 \quad (1)$$

$$C_xH_y + (x + y/4)O_2 \rightarrow xCO_2 + (y/2)H_2O \quad (2)$$

$$NO + CO \rightarrow CO_2 + (1/2)N_2 \quad (3)$$

$$(2x + y/2)NO + C_xH_y \rightarrow xCO_2 + (y/2)H_2O + (x + y/4)N_2 \quad (4)$$

Reactions (1) and (2) are catalysed by Pt and Pd, whereas Rh is mainly involved in NO_x reductions reactions ((3) and (4)). The reduction of NO with CO can yield N_2O instead of N_2:

$$2NO + CO \rightarrow N_2O + CO_2 \quad (5)$$

Cant et al. [8] studied the formation of N_2O in model Rh, Pd and Pt catalysts under a simulated gasoline exhaust with $CO + NO + C_3H_6 + C_3H_8 + H_2 + O_2$. Rh yielded the highest amount of N_2O, with maximum production between 250 and 400 °C. Pt yielded N_2O in a narrow range of temperatures around 400 °C, and Pd produced N_2O in two temperature ranges, below 200 °C and above 300 °C.

Other catalytic converters that yield N_2O, which are under development for Diesel vehicles [9], are those based on Pt catalysts for the Selective Catalytic Reduction (SCR) of NO_x with hydrocarbons. The pollutants emitted by diesel engines are soot, NO_x, CO and HC [10]. The concentrations of CO and HC in diesel exhausts are significantly lower than those emitted by a gasoline engine, NO_x and soot being the main pollutants. Diesel engines operate with O_2 excess, which results in high levels of O_2 in the exhaust (10–20%). The high concentration of O_2 hinders NO_x removal, since NO_x reduction cannot be performed with the reducing species

* Corresponding author. Tel.: +34 965 90 34 00x2226; fax: +34 965 90 34 54.
E-mail address: agus@ua.es (A. Bueno-López).

0926-3373/$ – see front matter © 2010 Elsevier B.V. All rights reserved.
doi:10.1016/j.apcatb.2010.02.034

present in the exhaust (HC and CO). Therefore, it is necessary to feed an additional reductant such as NH_3, urea, H_2, CO or HC [11]. A number of catalysts have been proposed for SCR with HC, and among them, the Pt group metals can be found. Burch and Millington [12] reviewed the behaviour of Pt, Pd, Rh, Ir and Ru in SCR of NO_x with HC, with particular reference to the formation of N_2O as by-product with some of these noble metals.

In spite of the noble metal/cerium oxide catalysts have been deeply studied for NO_x removal both under diesel and gasoline exhaust conditions, the N_2O decomposition mechanisms on these systems are not completely understood. One of the issues to be studied is the cerium oxides role in noble metal-catalysed N_2O decomposition. The purpose of this work is to analyse the decomposition of N_2O on Rh, Pd and Pt catalysts, devoting particular attention to the effect of the support on the activity of the noble metals for this reaction. The supports studied are γ-Al_2O_3 and different cerium oxides including pure CeO_2 and La- or Pr-doped CeO_2.

2. Experimental

2.1. Catalyst preparation

CeO_2 and 10 wt.% La- or Pr-doped CeO_2 supports were prepared from $Ce(NO_3)_3{\cdot}6H_2O$ (Aldrich, 99.9%), $La(NO_3)_3{\cdot}6H_2O$ (Merck, 99.9%) and $Pr(NO_3)_3{\cdot}6H_2O$ (Aldrich, 99.9%). The required amounts of these precursors were mixed in a mortar and calcined in static air at 600 °C for 90 min (heating rate 10 °C/min). The pure, La-doped and Pr-doped ceria supports are denoted by CeO_2, CeO_2(La) and CeO_2(Pr), respectively. Commercial γ-Al_2O_3 pellets by Across were crushed and the fine powder obtained was also used as support. This support is denoted by γ-Al_2O_3.

The four supports were impregnated with $Rh(NO_3)_3$ (Sigma–Aldrich, 99.9%), $Pt(NH_3)_4(NO_3)_2$ (Sigma–Aldrich, 99,995%) or $Pd(C_2H_3O_2)_2$ (Sigma–Aldrich, 99.98%) dissolved in water, dried at 200 °C and calcined at 500 °C for 2 h. The noble metal target content was 0.5 wt.% after calcination. The catalysts are referred to as "Rh, Pt or Pd" before the support notation.

2.2. Characterisation of supports and catalysts

Raman spectra of the supports were recorded in a Bruker RFS 100/S Fourier Transform Raman Spectrometer with a variable power Nd-YAG laser source (1064 nm). The laser beam was focused on the sample in a 180° backscattering configuration and 64 scans at 85 mW laser power (70 mW on the sample) were recorded. No sample heating was observed under these conditions.

X-ray diffractograms of the supports were recorded in a Bruker D8 advance diffractometer, using Cu Kα radiation (λ = 0.15418 nm). The diffractograms were recorded between 20 and 80° (2θ) with a step of 0.02° and a time per step of 3 s. The average crystallite size (D) of the supports was determined using the Scherrer's and Williamson–Hall's equations. In the Scherrer's equation:

$$D = \frac{K \cdot \lambda}{\beta \cdot \cos\theta}$$

λ is the X-ray wavelength, K is the particle shape factor, taken as 0.94 [13], β was defined as the width at half maximum of the peak and θ is the position (angle) of the peak.

The Williamson–Hall's equation (W–H) separates the effects of size and strain in the nanocrystals, using the equation:

$$\beta_{Total} = \beta_{Size} + \beta_{Strain} = \frac{0.9 \cdot \lambda}{D \cdot \cos\theta} + \frac{4 \cdot (\Delta d) \cdot \sin\theta}{d \cdot \cos\theta}$$

where β_{Total} is the full width half maximum of the XRD peak, λ is the incident X-ray wave length, θ is the position of the peaks, D is the crystallite size, and Δd is the difference of the d spacing corresponding to a typical peak. A plot of $\beta_{Total}{\cdot}\cos\theta$ versus $4{\cdot}\sin\theta$ yields the crystal size from the intercept value.

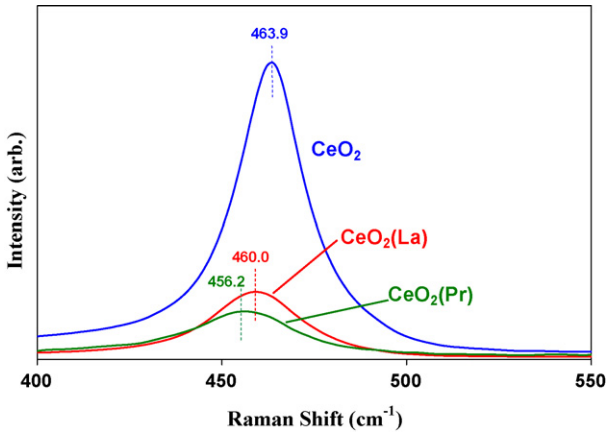

Fig. 1. Raman spectra of the cerium oxide supports.

The BET surface area of the supports was determined by physical adsorption of N_2 at −196 °C in an automatic volumetric system (Autosorb-6, Quantachrome).

A JOEL (JEM-2010) microscope, equipped with an EDS analyser (OXFORD, model INCA Energy TEM100), was used to obtain TEM images of the catalysts. Few droplets of an ultrasonically dispersed suspension of each catalyst in ethanol were placed in a copper grid with lacey carbon film and dried at ambient conditions for TEM characterisation. The size of the noble metal particles was measured by TEM with the software DigitalMicrograph, version 1.8.

Temperature programmed reduction by H_2 (H_2-TPR) of the catalysts was carried out in a Micromeritics Pulse ChemiSorb 2705 device, consisting of a tubular quartz reactor (inner diameter 5 mm) coupled to a thermal conductivity detector (TCD). The experiments were conducted with 20 mg of fresh catalyst. The sample was heated at 10 °C/min from room temperature to 1050 °C in 30 ml/min flow of 5 vol.% H_2 in Ar. A cold trap was placed before the TCD, consisting of a mixture of isopropyl alcohol and liquid nitrogen (temperature −89 °C). In order to quantify the total amount of H_2 consumed, CuO was used as calibration reference.

2.3. N_2O decomposition tests

N_2O decomposition tests were performed in a cylindrical fixed-bed reactor of 10-mm i.d. at atmospheric pressure. 100 mg of catalyst diluted with 700 mg of SiC were used, and the total flow rate was 100 ml/min (GHSV = 10,000 h^{-1}). N_2O decomposition tests were carried out under different gas streams: 1000 ppm N_2O/He; 1000 ppm N_2O/5% O_2/He or 1000 ppm N_2O/1000 ppm CO/He. The experiments consisted of point-by-point isothermal reactions in the range of 200–400 °C, which were extended until the steady state was reached. The gas composition was analysed by a HP 6890 gas chromatograph equipped with a TCD and two columns (Porapak Q, for N_2O and CO_2, and Molecular Sieve 13X, for O_2, N_2 and CO).

3. Results and discussion

3.1. Characterisation of the supports by Raman spectroscopy, XRD and N_2 adsorption

The structure of the cerium oxide supports has been studied by Raman spectroscopy (Fig. 1) and XRD (Fig. 2), both techniques providing complementary information. In one hand, XRD is a mass analysis technique giving information about more than 1 μm thickness, while Raman spectroscopy usually analyses about 10–100 nm.

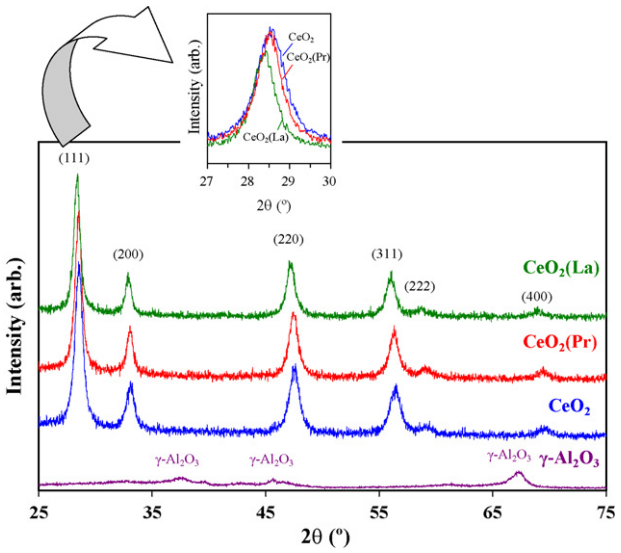

Fig. 2. XRD patterns of the supports.

On the other hand, Raman spectra of cerium oxides are caused by oxide anions vibration, while XRD is sensitive to the position of cations in the lattice [16].

Ceria-based materials present fluorite structure, based on a face-centered cubic cell, and this structure shows a characteristic Raman band at ca. 465 cm^{-1} assigned to the F_{2g} mode [13–15]. This band is identified in all the Raman spectra included in Fig. 1. Evidences of the presence of La_2O_3 or other species of La or Pr are not observed in Fig. 1, suggesting that La and Pr cations do not form segregated phases [17]. The presence of dopants deforms the lattice and reduces the intensity of the F_{2g} band [18], as observed in Fig. 1 for samples CeO_2(La) and CeO_2(Pr) with regard to pure CeO_2. The shift in the position of the F_{2g} band in doped samples with regard to pure CeO_2 is another evidence of the incorporation of dopants within the ceria lattice [19–21]. The cation La^{3+} (1.16 Å) is larger than the cation Ce^{4+} (0.97 Å), and therefore, the shift of the F_{2g} band towards lower frequencies in CeO_2(La) with regard to CeO_2 could be consequence of the lattice expansion. On the contrary, the cations Ce^{4+} and Ce^{3+} (0.97 and 1.14 Å, respectively) have very similar size than their counterpart Pr^{4+} and Pr^{3+} (0.96 and 1.13 Å, respectively). In this case, the shift of the F_{2g} band due to Pr doping must be attributed to alterations in the length and/or frequency of vibration of the metal-oxygen bonds, and not to changes in the size of the unit cell.

Fig. 2 shows the XRD patterns of the different supports. The alumina support shows characteristic peaks of γ-Al_2O_3, and the low intensity and broad width of the peaks reveal the low degree of crystallinity of this material. The diffractograms of pure and doped ceria samples present the reflections characteristic of solids with fluorite structure, corresponding to the planes (1 1 1), (2 0 0), (2 2 0), (3 1 1) (2 2 2) and (4 0 0) [20]. In agreement with the Raman spectroscopy results, XRD neither shows peaks assignable to La_2O_3 or other La or Pr species [17], that is, there are not evidences of phase segregation by these techniques.

The detailed analysis of the position of the XRD peaks provides additional information about the structure of the ceria supports. As shown in the zoom in of the peak (1 1 1), the position of the peak shifts toward lower angles when ceria is doped by La^{3+} because of the expansion of the unit cell [19–21]. In the case of Pr doping, the position of the peak (1 1 1) does not change significantly because, as previously mentioned, the Ce^{4+} and Ce^{3+} sizes are similar to those of Pr^{4+} and Pr^{3+}, respectively. The lattice parameters estimated for the pure and doped ceria sample, included in Table 1, support these conclusions. The lattice parameters for Pr doped ceria and pure ceria are quite similar (0.5420 and 0.5413 nm, respectively), and this confirms that the size of the unit cell is almost equal. On the contrary, the expansion of the unit cell by La doping leads to a higher lattice parameter (0.5439 nm for CeO_2(La)). The conclusions obtained by XRD about the effect of La and Pr doping in the ceria structure are consistent with the Raman spectroscopy conclusions.

Table 1
Supports characterisation data obtained by XRD and N_2 adsorption isotherms.

Support	Crystallite size by Scherrer (nm)	Crystallite size by W–H (nm)	Lattice constant (nm)	BET (m^2/g)
γ-Al_2O_3	–	–	–	78
CeO_2	11	13	0.5413	76
CeO_2(La)	14	20	0.5439	49
CeO_2(Pr)	13	17	0.5420	44

Table 1 also includes the average crystallite sizes of the ceria supports obtained from the X-ray diffractograms by using the Scherrer's and Williamson–Hall's equations. In the case of the alumina support, the crystal size could not be estimated due to the low crystallinity of this material. The BET area of the supports, as determined from N_2 adsorption isotherms, is also included in Table 1. The BET areas of the supports γ-Al_2O_3 and CeO_2 are similar (78 and 76 m^2/g, respectively), and the introduction of dopants in the CeO_2 structure reduces the area. This area reduction in doped ceria samples is consistent with the increase in the average crystallite size from 13 nm for pure CeO_2 to 17–20 nm for the doped supports, as calculated by the Williamson–Hall's equation. The promoting effect of La or Pr in ceria sintering only takes place at relatively moderate calcinations temperature (at 600 °C in this study). It has been observed that, at higher temperatures (800–1000 °C), La and Pr partially hinder crystal growth [22].

It is useful to compare the crystallite sizes obtained by applying the Scherrer's equation with those obtained with the Williamson–Hall's equation, because evidences about the formation of mixed oxides can be deduced from such comparison. The Scherrer's equation predicts similar crystallite sizes for the three CeO_2 supports (11–14 nm). This model assumes that the peak broadening is only due to the size of the crystallites, and the crystallite size values obtained are inconsistent with the BET values. On the contrary, the Williamson–Hall's equation, which takes into account that the creation of crystalline defects also affects the peaks width, indicates that the crystallite sizes of the doped samples are larger than that of pure CeO_2. The Williamson–Hall's sizes are consistent with the decrease of BET areas for doped samples in comparison with pure CeO_2. In this case, the introduction of La or Pr dopants in the ceria lattice is responsible of the creation of crystalline defects. Therefore, the better results obtained with the Williamson–Hall's equation in comparison with those obtained with the Scherrer's equation is another evidence of the introduction of La and Pr dopants within the ceria lattice.

3.2. Characterisation of the noble metals particle size by TEM

TEM has been used to analyse the noble metal particle size. Selected TEM pictures are compiled in Fig. 3 where, in most cases, the noble metal particles can be distinguished from the support. Noble metal particles are properly distinguished in samples with alumina support, because the atomic weights of aluminium and noble metals are very different. However, the noble metal particles are sometimes hardly distinguished when supported on cerium oxides. This is because the molecular weigh of both noble and internal transition metals is high, and therefore, their colour contrast is low. For this reason, and also because the loading is low

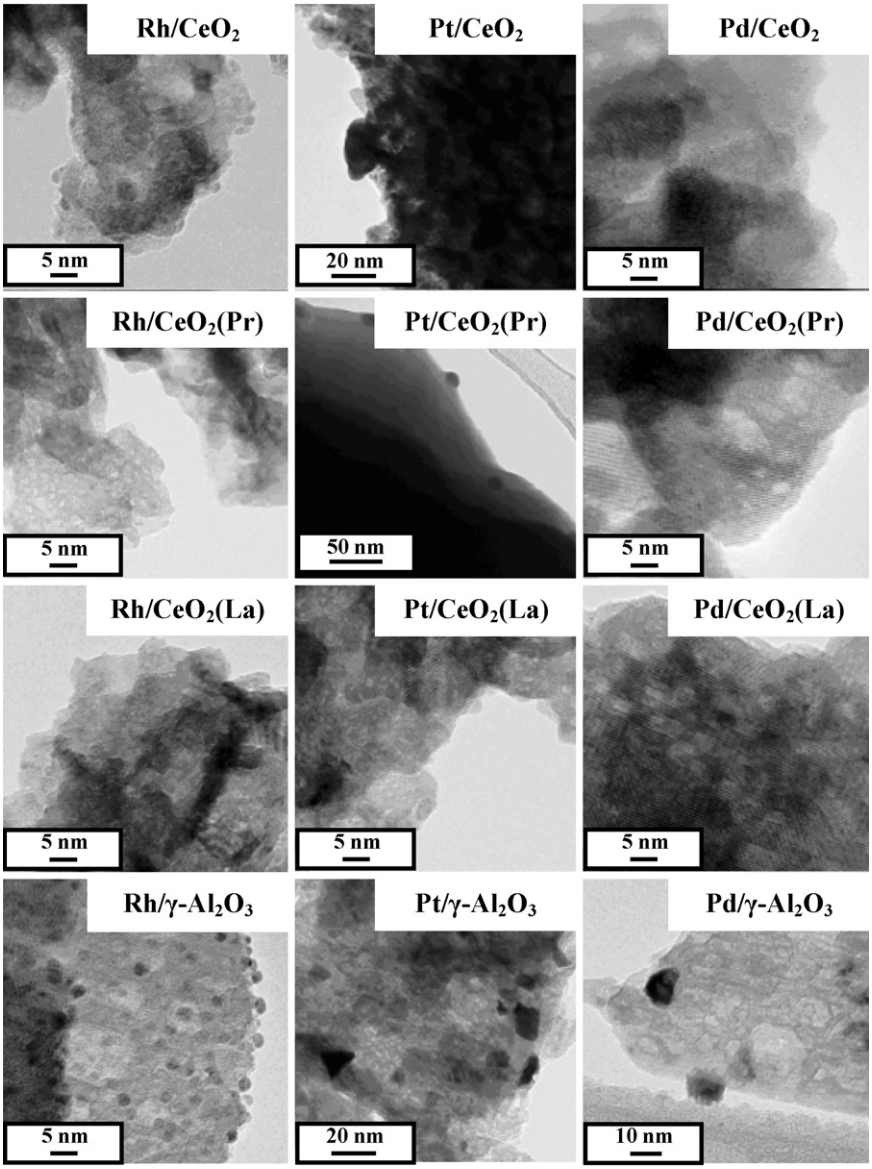

Fig. 3. TEM micrographs of the catalysts.

(0.5 wt.%), the noble metal particle size distribution cannot be properly obtained, since the number of noble metal particles identified is not high enough to get statistical significance. The size of the noble metal particles has been estimated with the data available for each catalyst, and Table 2 compiles the average particle size along with the size of the largest and smallest particle identified in each catalyst, which provides information about the degree of heterogeneity of the noble metal particles.

Table 2
TEM-characterisation of the noble metals particle size.

Catalyst	Average particle size (nm)	Minimum particle size (nm)	Maximum particle size (nm)
$Rh/\gamma\text{-}Al_2O_3$	2.3	1.2	3.1
Rh/CeO_2	2.2	1.1	4.9
Rh/CeO_2(La)	1.1	0.6	2.0
Rh/CeO_2(Pr)	1.2	0.6	1.9
$Pt/\gamma\text{-}Al_2O_3$	4.3	2.4	31.7
Pt/CeO_2	29.2	10.1	41.3
Pt/CeO_2(La)	–	–	–
Pt/CeO_2(Pr)	18.2	11.1	24.2
$Pd/\gamma\text{-}Al_2O_3$	12.0	1.2	24.2
Pd/CeO_2	<0.5	<0.5	<0.5
Pd/CeO_2(La)	<0.5	<0.5	<0.5
Pd/CeO_2(Pr)	<0.5	<0.5	<0.5

There are not significant differences among rhodium particle size on catalysts $Rh/\gamma\text{-}Al_2O_3$ and Rh/CeO_2, with an average size of 2.2–2.3 nm. Rhodium is slightly better dispersed on La or Pr-doped CeO_2 than on the pure oxide supports, and the average particle sizes are 1.1 and 1.2 nm for Rh/CeO_2(La) and Rh/CeO_2(Pr), respectively. The size of the largest and smallest rhodium particles identified on each catalyst suggests a narrow particle size distribution in all rhodium samples.

Among the Pt catalysts, the smallest average particle size of Pt is obtained with $\gamma\text{-}Al_2O_3$ as support (4.3 nm). Pt particles on Pt/CeO_2 and Pt/CeO_2(Pr) are larger (average sizes of 29.2 and 18.2 nm, respectively) and present very heterogeneous size distributions, as deduced from the very different values of the smallest and largest Pt particles identified in both catalysts. Pt particles have been hardly observed on the catalyst Pt/CeO_2(La), and this fact is attributed to experimental limitations related to the low colour contrast between the noble metal and support. However, the presence of Pt on this samples was confirmed by EDX analysis, and the

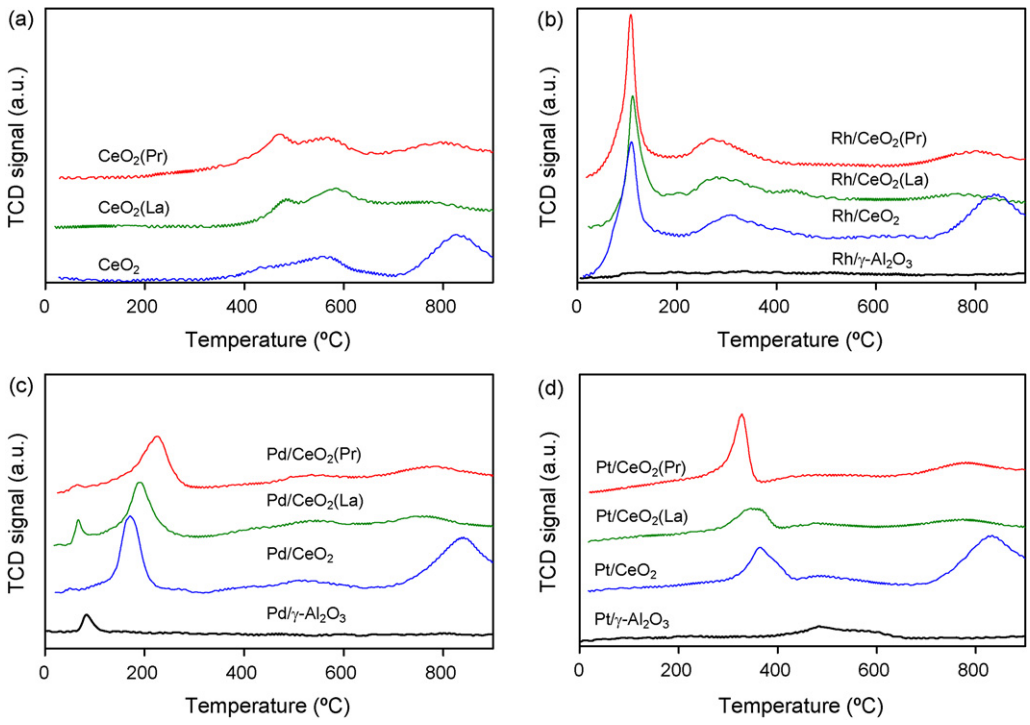

Fig. 4. H_2-TPR profiles for (a) supports, (b) Rh catalysts, (c) Pd catalysts, and (d) Pt catalysts.

Pt particle size on CeO_2(La) and CeO_2(Pr) supports are expected to be not very different.

The size of Pd particles depends significantly on the support used. The Pd particles on Pd/γ-Al_2O_3 present a very heterogeneous size distribution, ranging between 1.2 and 24.2 nm with an average particle size of 12 nm. However, a very high Pd dispersion is obtained on pure and doped ceria supports, being difficult to identify the Pd particles in the TEM pictures of these catalysts because of their small size. It is not possible to estimate the Pd particles size on ceria supports, but it can be ensured that it is lower than 0.5 nm. The presence of Pd in all ceria samples was confirmed by EDX analysis.

3.3. Samples characterisation by H_2-TPR

The reducibility of the different samples has been analysed by Temperature Programmed Reduction experiments with H_2 (H_2-TPR) and the profiles obtained are shown in Fig. 4. Fig. 4a shows the results obtained for the supports. Typically, the ceria reduction profiles are characterised by two main peaks [23]: the first one, at temperatures around 500 °C, is attributed to the reduction of surface Ce^{4+} and the second peak, at temperatures around 850 °C, is assigned to the reduction of bulk Ce^{4+}. This type of profile is evident in sample CeO_2. However, the La- and Pr-containing samples do not show the peaks described but a broad band where surface and bulk reduction cannot be clearly distinguish to each other. This type of broad profile is an evidence of the high mobility of oxygen in the lattice of the doped ceria samples [24]. The improvement in the ceria support reducibility upon La or Pr doping confirms the conclusions drawn from the XRD and Raman spectroscopy characterisation, where it was observed that the dopants are incorporated into the lattice of ceria. However, in spite of the H_2-TPR profiles of CeO_2(La) and CeO_2(Pr) are characterised by broad bands, several peaks can be identified along those which can be attributed to particular events. The reduction profile of CeO_2(Pr) shows a small peak with maximum at 475 °C which may be attributed to the reduction of Pr^{4+} to Pr^{3+} (note that Pr^{4+} can be reduced more easily than Ce^{4+} [25]). CeO_2(La) also presents a small peak with maximum at 490 °C, but considering that La^{3+} is not reducible under the conditions employed and the strong CO_2 chemisorption capacity of lanthanum oxide, this peak is tentatively attributed to the desorption of chemisorbed species, most probably CO_2. The peaks at 575 and 800 °C laying on the broad profiles of CeO_2(La) and CeO_2(Pr) could be related with the preferential reduction of surface and bulk Ce^{4+} cations, respectively.

The H_2-TPR profiles are not significantly modified in the range of temperatures where supports bulk reduction takes place ($T > 700$ °C, approximately) after noble metals loading, neither for pure ceria nor for La- and Pr-doped samples. On the contrary, noble metals significantly modify the TPR profiles at low and mild temperature. The onset temperature for the noble metal-free ceria supports is about 375 °C, and the noble metal-containing ceria samples show H_2 consumption at much lower temperature. The lowest temperatures are achieved with Rh (Fig. 4b), for which two low-temperature peaks centred at about 110 °C and 275–300 °C are observed. The lowest temperature peak is attributed to noble metal-catalysed surface reduction of the ceria supports [26], which is confirmed by quantifying the amount of H_2 consumed in this peak. This amount is much higher than that necessary to reduce all the noble metal on the catalysts, and therefore, the support reduction can be inferred. For example, the amount of H_2 consumed in the lowest temperature peak of the Rh/CeO_2 sample is that required to reduce 6.5 times the amount of rhodium on this catalyst, which confirms that the ceria support is being reduced at this temperature. In this sense, some authors [27,28] have observed that some noble metals can be reduced with H_2 at room temperature or even below the ambient temperature. This would explain the absence of noble metal reduction peaks in some catalysts with γ-Al_2O_3 support, because the TCD signal was stabilised for 30 min at room temperature before heating.

The reduction peak centred at 275–300 °C for the Rh-containing samples (Fig. 4b) is also attributed to surface reduction of the cerium oxide supports. However, in this case, the catalytic effect of the noble metal is lower than in the peak at 110 °C. This is attributed

to ceria reduction without close contact with the noble metal [26]. Some authors have suggested that the decomposition of surface carbonates or carbonates occluded within the CeO_2 structure may also contribute to the TCD signal in this range of temperature (around 275–300 °C) [29,30].

The reduction of the cerium oxide supports surface occurs at temperatures around 180–230 °C for Pd-containing samples (Fig. 4c), and at 330–370 °C for Pt samples (Fig. 4d). Taking into account the low-temperature peaks, the catalytic activity of the noble metals to accelerate the reduction of the cerium oxide supports surface follows the trend Rh > Pd > Pt. As it will be shown afterwards, the support reducibility plays an important role in the catalytic decomposition of N_2O.

3.4. Catalytic tests

3.4.1. Catalytic N_2O decomposition

Fig. 5 shows the N_2O decomposition profiles obtained in catalytic tests conducted with 1000 ppm N_2O/He. The results obtained with Rh catalysts and bare supports are compiled in Fig. 5a, and those with Pd and Pt catalysts in Fig. 5b and c, respectively. Note that the non-catalytic decomposition of N_2O into N_2 and O_2 requires about 625 °C to occur in a measurable extent [1]. The noble metal-free supports (Fig. 5a) have a very low catalytic activity below 500 °C, and for instance, only 10% N_2O decomposition is reached at this temperature with pure CeO_2. The catalytic activity increases for the noble metal-containing samples in comparison with the bare supports, and Rh (Fig. 5a) is the most active noble metal among those tested. Rh catalysts (Fig. 5a) are active for N_2O decomposition from 200 to 250 °C, depending on the support, and the complete conversion is reached in the range 300–400 °C. The activity of Rh catalysts for N_2O decomposition follows the trend:

$$Rh/CeO_2(Pr) > Rh/CeO_2(La) > Rh/CeO_2 > Rh/\gamma\text{-}Al_2O_3$$

Both the pure and doped ceria supports improve the catalytic activity of Rh in comparison with that of γ-Al_2O_3-supported Rh. Considering the similar size of the rhodium particles in all the catalysts (see sizes on Table 2), the sequence in activity observed has to be due to the effect of metal-support chemical interactions. The improved catalytic activity of Rh when supported on a cerium oxide carrier could be related with the redox properties of these oxides. The lowest activity of the Rh/γ-Al_2O_3 catalyst, among those with Rh, could be consequence of the non-reducibility of alumina under reaction conditions. This hypothesis is supported by the conclusions of a previous study [31], where a linear relationship between the catalytic activity for N_2O decomposition and the reducibility of the support surface was obtained for a set of ceria supported Rh samples, the easier the reduction, the higher the activity. This relationship was demonstrated by testing nine different ceria supports, both pure and doped, with very different physical–chemical properties.

Pd (Fig. 5b) and Pt (Fig. 5c) catalysts are much less effective for N_2O decomposition than those of Rh, and they are not able to reach 100% conversion in the range of temperature studied. In Pt catalysts (Fig. 5c), the effect of the support is difficult to be interpreted. The catalytic activity of Pt/CeO_2 is higher than that of Pt/γ-Al_2O_3, while the catalytic activity of Pt supported on La- and Pr-doped ceria diminishes in comparison to Pt/γ-Al_2O_3. For Pd catalysts, all the samples with either pure or doped ceria support showed similar activity, this being higher than that of Pd/γ-Al_2O_3. In one hand, the TEM-estimated size of the Pd particles supported on pure and doped cerias (<0.5 nm in all cases) are much smaller than that of Pd supported on γ-Al_2O_3 (12 nm average size), which could explain the catalytic activity differences among Pd samples. However, it cannot be excluded that the redox properties of the ceria supports could also improve the activity of Pd for N_2O decomposition in comparison with γ-Al_2O_3 in a certain extent. All the Pd samples with ceria supports, either bare or doped, behave equal in catalytic tests (Fig. 5b) while differences in the redox properties among the pure and doped ceria supports were noticed (Fig. 4c). This suggests that the effect of Pd particle size on ceria supports (in comparison to γ-Al_2O_3) prevails against the potential improvement due to the redox properties of the cerium oxides.

In Fig. 6, the N_2O decomposition onset temperature, obtained from the Fig. 5 curves, has been plotted against the temperature of support surface reduction by H_2, obtained from Fig. 4. The N_2O decomposition onset temperature has been defined as the temperature required to decompose 10% of the N_2O fed to the reactor and the temperature of surface reduction by H_2 corresponds to the maximum of the lowest temperature H_2 reduction peak in H_2-TPR experiments (Fig. 4), which is attributed to the noble metal-catalysed reduction of the support. Fig. 6 shows some relation between the reducibility of the supports and the activity for N_2O decomposition of the noble metal/ceria catalysts. For instance, the most easily reduced catalysts are those with Rh, and they are

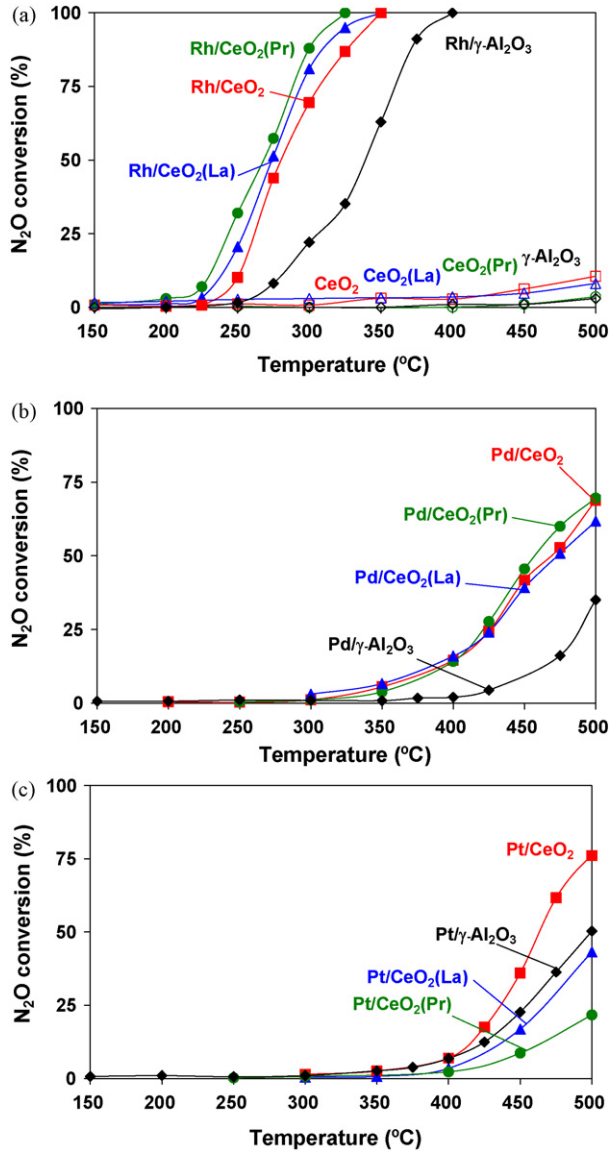

Fig. 5. N_2O conversion as a function of temperature for (a) supports and Rh catalysts, (b) Pd catalysts and (c) Pt catalysts.

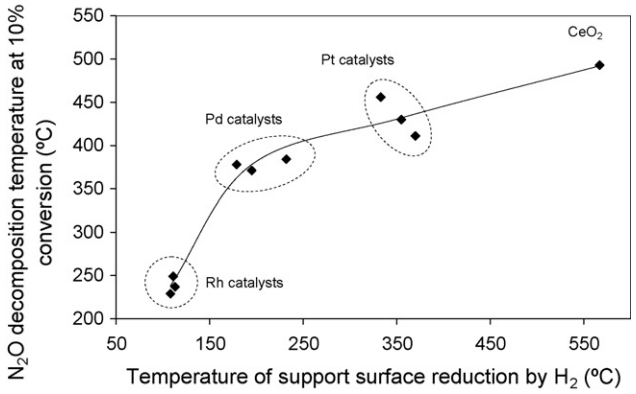

Fig. 6. N_2O decomposition onset temperature against temperature for cerium oxide supports surface reduction by H_2.

also the most active catalysts. Both the catalytic activity for N_2O decomposition and for catalytic reduction by H_2 of the support surface follow the trend Rh > Pd > Pt, suggesting that the rate-limiting step of the N_2O decomposition mechanism is the reduction of the catalytic active sites. However, the effect of the redox properties of the ceria supports on the catalytic activity for N_2O decomposition is evident for Rh catalysts but it is not for Pd and Pt catalysts.

3.4.2. *Catalytic removal of N_2O under oxidising ($N_2O + O_2$) and reducing ($N_2O + CO$) conditions*

To deep into the analysis of the role of the redox processes in the N_2O decomposition on noble metal/ceria catalysts, catalytic tests have been carried out under oxidising ($N_2O + O_2$) and reducing ($N_2O + CO$) conditions. For these experiments, the noble metal catalysts with CeO_2(Pr) support have been selected. Fig. 7 shows the N_2O conversion curves for the different experiments performed with these catalysts under 1000 ppm N_2O + 5%O_2/He ($N_2O + O_2$), and 1000 ppm N_2O + 1000 ppm CO/He ($N_2O + CO$). The experiments conducted with 1000 ppm N_2O/He (N_2O) have been also included for comparative purposes. The analysis of the reaction products confirms that N_2O is decomposed into N_2 and O_2 in experiments performed in the absence of CO, both with and without O_2 in the feed. In experiments conducted under $N_2O + CO$, and once the steady state is reached, N_2O reduction takes place with stoichiometric consumption of both CO and N_2O and stoichiometric formation of N_2 and CO_2.

O_2 partially inhibits the catalytic decomposition of N_2O over all the catalysts tested, as deduced by comparison of curves obtained under N_2O and $N_2O + O_2$ in Fig. 7. This is consistent with the relationship obtained in Fig. 6 between the activity of the noble metal/ceria catalysts for N_2O decomposition and the reducibility of the support, since O_2 hinders the reduction and therefore the activity. These results also evidence that the rate-limiting step of the N_2O decomposition mechanism is the reduction of the catalytic active sites, and the partial inhibition of the catalytic activity in the presence of O_2 supports this hypothesis. Kapteijn et al. [1] reported that O_2 inhibits the catalytic activity of most of the N_2O decomposition catalysts, in a different extent depending on the nature of the catalyst.

On the contrary, CO enhances significantly the conversion of N_2O on all the noble metal/CeO_2(Pr) catalysts tested, as deduced by comparison between the curves obtained under N_2O and $N_2O + CO$ (Fig. 7). This improvement is moderate for Rh/CeO_2(Pr) but is very important for the Pd and Pt catalysts. As observed in the H_2-TPR experiments (Fig. 4), the surface of the Rh/CeO_2(Pr) catalyst is reduced more easily than that of the counterpart Pd and Pt catalysts, that is, the easier is the reduction of the catalyst the lower is the

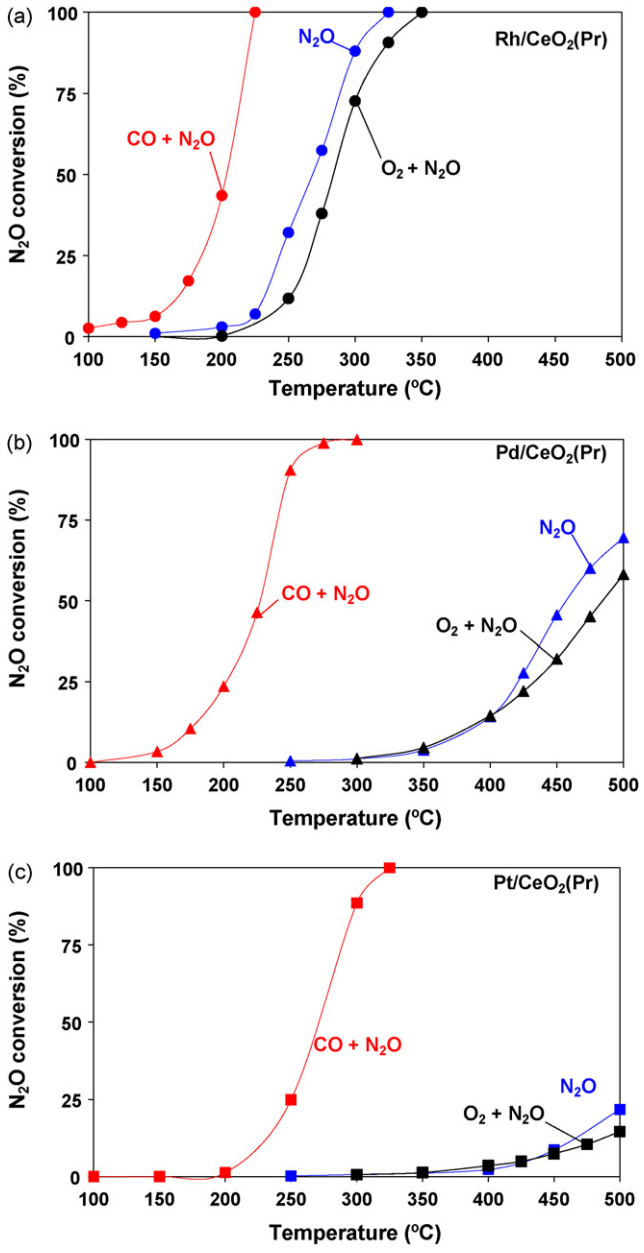

Fig. 7. Catalytic conversion of N_2O under 1000 ppm N_2O/He (N_2O), 1000 ppm N_2O + 5%O_2/He ($N_2O + O_2$), and 1000 ppm N_2O + 1000 ppm CO/He ($N_2O + CO$) with the catalysts (a) Rh/CeO_2(Pr), (b) Pd/CeO_2(Pr) and (c) Pt/CeO_2(Pr).

effect of CO during the catalytic removal of N_2O. The catalytic tests performed under $N_2O + CO$ suggest once more that the rate-limiting step of the N_2O decomposition mechanism is the reduction of the active sites of the catalysts, and that CO accelerates the reduction.

Arrhenius plots, which are included in Fig. 8, have been drawn for the experiments performed under the N_2O atmosphere for the noble metal catalysts with CeO_2(Pr) or γ-Al_2O_3 supports and, additionally, for the for N_2O removal in the presence of O_2 or CO by the noble metal/CeO_2(Pr) catalysts. Suitable straight lines have been obtained for all the experiments and apparent activation energies have been calculated from these plots. All the values obtained are lower than those reported for the non-catalytic N–O bond splitting in the N_2O molecule (250–270 kJ/mol) [32–34].

In the absence of CO and O_2, the most significant result is the difference in the apparent activation energies for Rh/γ-Al_2O_3 and Rh/CeO_2(Pr), 145 and 91 kJ/mol, respectively. This difference sug-

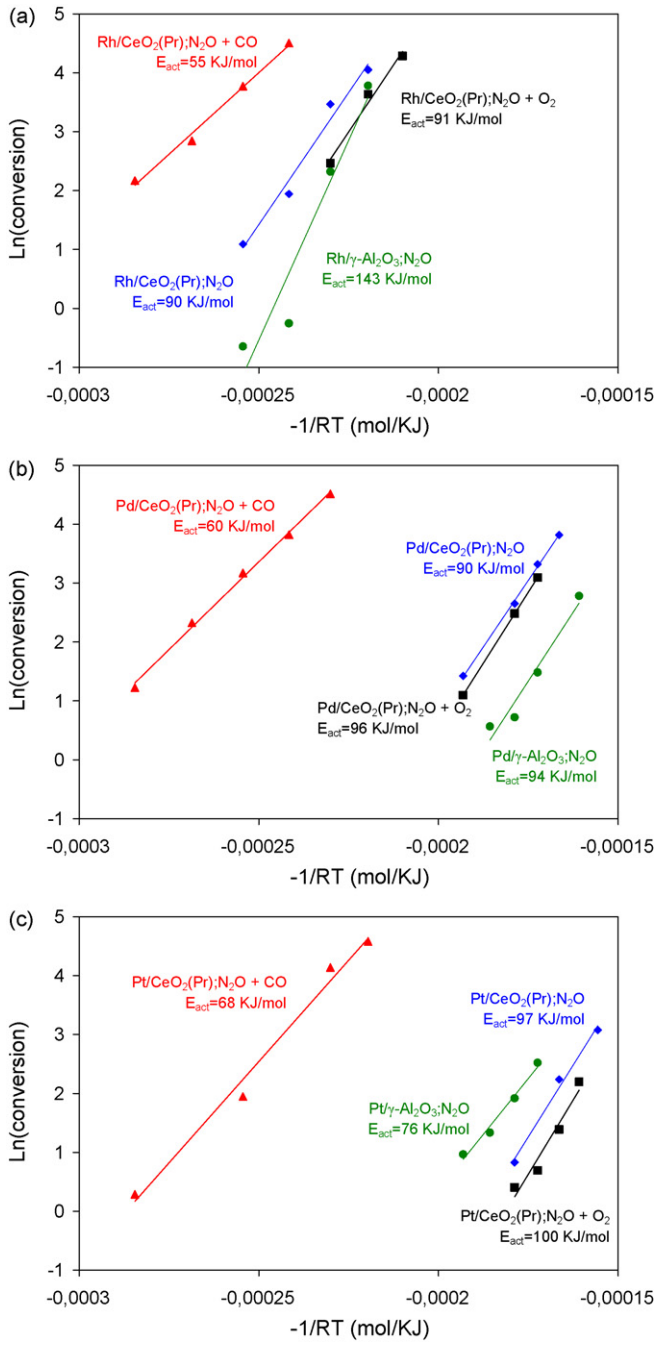

Fig. 8. Arrhenius plots for the decomposition/reduction of N_2O in different atmospheres for (a) Rh catalysts, (b) Pd catalysts and (c) Pt catalysts.

gests a different reaction mechanism and the participation of the CeO_2(Pr) support in such reaction mechanism.

On the other hand, for catalysts with CeO_2(Pr) support, the addition of O_2 to the gas stream does not change the apparent activation energy, and values in the range 91–100 kJ/mol were obtained. This supports that O_2 neither changes the N_2O decomposition mechanism nor the rate-limiting step of the catalytic N_2O decomposition. It has been previously proposed that O_2 inhibits partially the activity for N_2O decomposition of the noble metal/ceria catalysts because hinders the reduction of active sites. The similar activation energy values obtained for the catalytic N_2O decomposition reactions with and without O_2 in the stream supports this hypothesis.

On the contrary, for noble metal/CeO_2(Pr) catalysts, the apparent activation energies decrease from 90 to 97 kJ/mol for the catalytic N_2O decomposition to 55–68 kJ/mol for the N_2O–CO reaction. This decrease in the apparent activation energies supports that CO accelerates the rate-limiting step of the mechanism, which seems to be the reduction of the catalysts active sites.

3.5. Discussion on the N_2O decomposition mechanism

Considering both the results obtained in this study and the N_2O decomposition mechanisms described in the literature for different catalysts [1], it is proposed that the decomposition of N_2O over the Rh, Pd and Pt catalysts tested in the current study occurs with the successive reduction and oxidation of noble metal active sites by N_2O molecules (Eley–Rideal mechanism):

$$NM*\text{-}O + N_2O \rightarrow NM* + N_2 + O_2 \quad \text{(Step 1)}$$

$$NM* + N_2O \rightarrow NM*\text{-}O + N_2 \quad \text{(Step 2)}$$

where "NM*" and "NM*-O" are reduced (not necessarily NM(0) state) and oxidised noble metal active sites, respectively.

Besides these two steps, it has to be also considered another O_2 formation pathway, consisting of the recombination of two oxygen atoms located in two oxidised sites (Langmuir–Hinshelwood mechanism):

$$2NM*\text{-}O \rightarrow 2NM* + O_2 \quad \text{(Step 3)}$$

The participation of the noble metals in the N_2O decomposition mechanism is confirmed by the fact that the noble metal-free supports have very low or null activity under the experimental conditions of the current study (see Fig. 5a).

However, it is reasonable to think that the reaction mechanism is more complex than that described by steps 1–3. For example, it can be assumed that steps 1 and 2 are a combination of steps involving dissociative chemisorption of N_2O or molecular chemisorption followed by dissociation of N_2O molecules. Also, the experimental evidences obtained for the Rh catalysts about the relationship between the ceria supports reducibility and catalytic activity (Fig. 6) and the differences in apparent activation energies among Rh catalysts with different supports (Fig. 8) suggest that, for this metal, the ceria supports participate in the N_2O decomposition mechanism. This participation could be related with the reoxidation of noble metal active sites with oxygen from ceria support following a sequence of reactions described by steps 4 and 5:

$$NM* + Ce*\text{-}O \rightarrow NM*\text{-}O + Ce* \quad \text{(Step 4)}$$

$$Ce* + N_2O \rightarrow Ce*\text{-}O + N_2 \quad \text{(Step 5)}$$

In these reactions, "Ce*" is a reduced active site of the ceria support, most probably associated with an oxygen vacancy link to a Ce^{3+} cation (or Pr^{3+} in the support CeO_2(Pr)), and "Ce*-O" is an oxidised active site on the ceria support that is able to transfer oxygen to the noble metal. The transfer of oxygen from ceria to the noble metal (step 4) leads to the local reduction of the support, which must restore the oxygen balance by reoxidation of the vacant sites created with oxygen of a N_2O molecule (step 5). Steps 4 and 5 are valid for catalysts with CeO_2-based supports, but not for catalysts with γ-Al_2O_3 support, since γ-Al_2O_3 is not able to involve its oxygen in the reaction mechanism. However, for Pd/CeO_2(Pr) and Pt/CeO_2(Pr) catalysts, their low catalytic activity for N_2O decomposition in comparison to that of the Rh/CeO_2(Pr) catalyst (see Fig. 5), as well as the similar apparent activation energy value for both ceria and alumina catalysts (see Fig. 8), suggest that steps 4 and 5 are not significant steps in the reaction mechanism for Pd and Pt.

The rate of each step of the described mechanism will depend on the nature of both the noble metal and the support. However, the

experimental data suggest that, in all cases, the rate-limiting step is the active sites reduction (steps 1 and/or 3). This is supported by several experimental evidences: (i) the relationship between catalytic activity for N_2O decomposition and H_2 reduction (Fig. 6), (ii) the partial inhibition of the catalytic activity by O_2 (Fig. 7), (iii) the improvement of N_2O decomposition in the presence of CO (Fig. 7) and (iv) the decrease of apparent activation energies for the reaction N_2O–CO in comparison to N_2O decomposition (Fig. 8).

In the presence of CO (Fig. 7), the active sites reduction accelerates the slow step of the mechanism:

$$NM* \text{-} O + CO \rightarrow NM* + CO_2 \quad \text{(Step 6)}$$

For catalysts with a ceria-based support, the partial reduction of the support by CO may also take place:

$$Ce* \text{-} O + CO \rightarrow Ce* + CO_2 \quad \text{(Step 7)}$$

The ceria support reduction by CO (step 7) will also enhance the N_2O decomposition rate, since the active sites created on the ceria supports upon CO reduction will be also involved in N_2O removal throughout the step 5.

The partial inhibition of the catalytic N_2O decomposition by O_2 (see Fig. 7) is attributed to the competition between N_2O and O_2 for the catalysts active sites (competition between steps 8 and 2). Either the sites located on the noble metal or those on the support (competition between steps 8 and 9 with steps 2 and 5) can be affected by O_2.

$$NM* + O_2 \rightarrow NM* \text{-} O_2 \rightarrow 2NM* \text{-} O \quad \text{(Step 8)}$$

$$Ce* + O_2 \rightarrow Ce* \text{-} O_2 \rightarrow 2Ce* \text{-} O \quad \text{(Step 9)}$$

In reactions 8 and 9 both the dissociative and the molecular chemisorption of O_2 could occur.

4. Conclusions

Rh, Pd and Pt have been supported on γ-Al_2O_3, pure CeO_2 and La- or Pr-doped CeO_2, and these catalysts have been tested for N_2O decomposition. The following conclusions have been drawn:

- The three noble metals tested (Rh, Pd and Pt) catalyse the decomposition of N_2O, Rh being the most active metal.
- In some cases, the redox properties of the support affect the catalytic activity. For Rh catalysts, those with a ceria-based support present higher activity than Rh/γ-Al_2O_3.
- A relationship between the activity for N_2O decomposition of the noble metal catalysts with a ceria-based support and the reducibility of the catalysts by H_2 has been found, the easier is the reduction the higher is the catalytic activity.
- The rate-limiting step of the N_2O decomposition mechanism over noble metal catalysts with a ceria-based support seems to be the reduction of the catalytic active sites. For Rh catalysts, it is evident that ceria supports, either pure or doped, are directly involved in the N_2O decomposition process, while ceria participation is not so evident for Pd and Pt catalysts.

Acknowledgment

The authors thank the project CIT-420000-2009-48, funded by the Spanish Ministry of Science and Innovation, and Generalitat Valenciana (PROMETEO/2009/047) for the financial support. S. Parres thanks her thesis grant to University of Alicante-CAM-Unión FENOSA.

References

[1] F. Kapteijn, J. Rodríguez-Mirasol, J.A. Moulijn, Appl. Catal. B 9 (1996) 25.
[2] J. Pérez-Ramírez, F. Kapteijn, K. Schoffel, J.A. Moulijn, Appl. Catal. B 44 (2003) 117.
[3] K. Yuzaki, T. Yarimizu, K. Aoyagi, S. Ito, K. Kunimori, Catal. Today 45 (1998) 129.
[4] G. Centi, S. Perathoner, F. Vazzana, M. Marella, M. Tomaselli, M. Mantegazza, Adv. Environ. Res. 4 (2000) 325.
[5] S. Imamura, R. Hamada, Y. Saito, K. Hashimoto, H. Jindai, J. Mol. Catal. A 139 (1999) 55.
[6] H.S. Gandhi, G.W. Graham, R.W. McCabe, J. Catal. 216 (2003) 433.
[7] P. Vidmar, P. Fornasiero, J. Kašpar, G. Gubitosa, M. Graziani, J. Catal. 171 (1997) 160.
[8] N.W. Cant, E. Dennys, D.C. Angove, Chambers, Appl. Catal. B 17 (1998) 63.
[9] G. Garrigós-Pastor, S. Parres-Esclapez, A. Bueno-López, M.J. Illán-Gómez, C. Salinas-Martínez de Lecea, Appl. Catal. A 354 (2009) 63.
[10] J.P.A. Neeft, M. Makkee, J.A. Moulijn, Fuel Process. Technol. 47 (1996) 1.
[11] B.A.A.L. Van Setten, M. Makkee, J.A. Moulijn, Catal. Rev. Sci. Eng. 43 (2001) 489.
[12] R. Burch, P.J. Millington, Catal. Today 26 (1995) 185.
[13] L.N. Ikryannikova, A.A. Aksenov, G.L. Markaryan, G.P. Murav'eva, B.G. Kostyuk, A.N. Kharlanov, E.V. Lunina, Appl. Catal. A 210 (2001) 225.
[14] J. Kašpar, P. Fornasiero, M. Grazini, Catal. Today 50 (1999) 285.
[15] A. Mineshige, T. Taji, Y. Muroi, M. Kobune, S. Fujii, N. Nishi, M. Inaba, Z. Ogumi, Solid State Ionics 135 (2000) 481.
[16] M. Fernández-García, A. Martínez-Arias, A. Iglesias-Juez, C. Belver, A.B. Hungria, J.C. Conesa, J. Soria, J. Catal. 194 (2000) 385.
[17] A. Bueno-López, K. Krishna, M. Makkee, J.A. Moulijn, J. Catal. 230 (2005) 237.
[18] J.R. Mcbride, K.C. Hass, B.D. Poindexter, W.H. Weber, J. Appl. Phys. 76 (1994) 2435.
[19] J.E. Spanier, R.D. Robinson, F. Zheng, S.W. Chan, I.P. Herman, Phys. Rev. B 64 (2001) 2454071.
[20] F. Zhang, S.W. Chan, J.E. Spanier, E. Apak, Q. Jin, R.D. Robinson, I.P. Herman, Appl. Phys. Lett. 80 (2002) 127.
[21] S. Rossignol, C. Descorme, C. Kappenstein, D. Duprez, J. Mater. Chem. 11 (2001) 2587.
[22] K. Krishna, A. Bueno-López, M. Makkee, J.A. Moulijn, Appl. Catal. B 75 (2007) 210.
[23] J.M. García Cortes, J. Pérez Ramírez, M.J. Illán Gómez, F. Kapteijn, J.A. Moulijn, C. Salinas Martínez de Lecea, Appl. Catal. B 30 (2001) 399.
[24] G.L. Markaryan, L.N. Ikryannikova, G.P. Muravieva, A.O. Turakulova, B.G. Kostyuk, E.V. Lunina, V.V. Lunin, E. Zhilinskaya, A. Aboukais, Colloids Surf. A 151 (1999) 435.
[25] K. Krishna, A. Bueno-López, M. Makkee, J.A. Moulijn, Appl. Catal. B 75 (2007) 189.
[26] J. Silvestre-Albero, F. Rodríguez-Reinoso, A. Sepúlveda-Escribano, J. Catal. 210 (2002) 127.
[27] P. Fornasiero, J. Kaspar, V. Sergo, M. Graziani, J. Catal. 182 (1999) 56.
[28] P. Fornasiero, J. Kaspar, T. Montini, M. Graziani, V. Dal Santo, R. Psaro, S. Recchia, J. Mol. Catal. A 204 (2003) 683.
[29] F.M.Z. Zotin, L. Tournayan, J. Varloud, V. Perrichon, R. Frety, Appl. Catal. A 98 (1993) 99.
[30] P. Fornasiero, R. DiMonte, G.R. Rao, J. Kaspar, S. Meriani, A. Trovarelli, M. Graziani, J. Catal. 151 (1995) 168.
[31] A. Bueno-López, I. Such-Basáñez, C. Salinas-Martínez de Lecea, J. Catal. 244 (2006) 102.
[32] K. Jones, in: J.C. Bailar, H.J. Emeleus, R. Nyholm, A.F. Trotman-Dickenson (Eds.), Comprehensive Inorganic Chemistry, Pergamon Press, Oxford, 1984, p. p. 316.
[33] W.M. Kalback, C.M. Sliepcevich, Ind. Eng. Chem. Fundam. 17 (1978) 165.
[34] B.G. Reuben, J.W. Linnett, Trans. Faraday Soc. 55 (1959) 1543.